# Transformations to and from the Gyroid Phase in a Diblock Copolymer

**M. E. Vigild,*,† K. Almdal, and K. Mortensen**

*Condensed Matter Physics and Chemistry Department, Risø National Laboratory, DK-4000 Roskilde, Denmark*

**I. W. Hamley***

*School of Chemistry, University of Leeds, West Yorkshire LS2 9JT, U.K*

**J. P. A. Fairclough‡ and A. J. Ryan‡**

*Manchester Materials Science Centre, UMIST, Grosvenor Street, Manchester M1 7HS, U.K., and CLRC Daresbury Laboratory, Warrington WA4 4AD, U.K*

*Received November 13, 1997; Revised Manuscript Received May 27, 1998*

ABSTRACT: Simultaneous small-angle scattering and in situ dynamic mechanical measurements offer an excellent opportunity to relate the macroscopic dynamical mechanical response of block copolymers and their mesoscopic structural behavior. We use small-angle neutron scattering and rheology to examine the ordered phases and the order−order transitions exhibited by a poly(ethylene-*alt*-propylene)−poly(dimethylsiloxane) diblock copolymer. An intermediate structure—very similar to the hexagonal perforated layer (HPL) phase reported in other diblock systems—proves to be metastable, and we study the kinetics and epitaxy of its relaxation to the "gyroid" phase of $Ia\bar{3}d$ symmetry. Likewise we study the relaxation of a supercooled hexagonal phase to the gyroid structure and also observe that the gyroid phase is bypassed in a slow cool from the hexagonal phase to the HPL-like structure. The origin of a typical scattering pattern obtained from a highly oriented crystal structure of a sample in the gyroid phase is investigated and related to real space projections of the gyroid morphology. Synchrotron small-angle X-ray scattering is used for high-resolution studies of the ordered phases. Reversibility of transitions between different mesoscopic structures is studied, especially to and from the gyroid phase, and puzzling patterns of the HPL-like structure are observed.

## Introduction

Recent observations[1−6] in low molar mass diblock copolymer melts of a bicontinuous cubic structure of $Ia\bar{3}d$ symmetry, resembling the "gyroid" structure observed for lyotropic liquid crystals,[7−9] highlight the complexity of phase behavior of these materials. This structure is the most commonly observed bicontinuous cubic phase for amphiphile solutions and is the only such phase observed to date for low molar mass block copolymers.[10] For consistency with earlier studies,[2,10−12] we will refer to it as the gyroid phase (G) in this paper. The gyroid phase has been observed between the lamellar (LAM) and hexagonal-packed cylinder (HEX) phases, close to the order−disorder transition (ODT)[3,4,13−16] as in surfactants. The stability of this phase has been accounted for theoretically using self-consistent mean field theory by Matsen and co-workers.[11,12] It is found to be stable for block copolymers in the weak and intermediate segregation regimes, although mean field theory does not account for the direct transition between the gyroid phase and the disordered, isotropic phase that is observed experimentally.[3,4,13−16] When composition fluctuations are included, following the method of Brazovskii, theory can account for this direct transition.[17,18] Furthermore, this direct transition is only predicted for block copolymers below a critical degree of polymerization.[18]

Transformations between ordered phases in block copolymer melts or surfactant solutions involve a large-scale reorganization of macromolecular aggregates composed of polymer chains or amphiphiles, respectively. It was shown that such transformations can occur epitaxially, in which case some structural elements of the second phase grow from the first, without long-range transport of material, while preserving the orientation of some layer planes.[1,8] Rançon and Charvolin observed epitaxial relationships between the LAM, G, and HEX phases on heating (fixed concentration) solutions of the surfactant hexaethylene glycol mono-*n*-dodecyl ether ($C_{12}E_6$) in water. The {211} planes of the gyroid structure were found to be epitaxially related to the {001} planes of the LAM phase and the {10} planes of the HEX phase.[8] Schultz et al. reported a similar epitaxial relationship between the HEX and gyroid phases in a blend of poly(styrene)−poly(2-vinylpyridine) diblock copolymers.[1,19]

Another class of complex phases reported in diblock copolymers is the perforated and modulated layer structures.[20−23] Hamley et al. observed such intermediate structures on heating between the LAM and HEX phases in a number of polyolefin diblock copolymers of moderate molar mass ($(4-15) \times 10^4$ g/mol).[20,21] An initial modulation of the lamellae (with hexagonal symmetry) appeared to develop into a hexagonal-perforated layer (HPL) structure. This structure resembles the "catenoid lamellar" phase[22] and "folded lace" structure[23] reported elsewhere. In more recent studies, Hajduk et al. have re-examined perforated and modulated layer structures in a wide range of diblock copolymer materials and shown that these morphologies

* To whom correspondence should be addressed.

† Current address: Department of Chemical Engineering and Materials Science, University of Minnesota, Minneapolis, MN 55455.

‡ Current address: Department of Chemistry, University of Sheffield, Sheffield SH3 7HF, U.K.

S0024-9297(97)01674-4 CCC: $15.00 
Published on Web 08/06/1998

**Table 1. Molecular Characteristics and Transition Temperatures of Polymers Studied**

| sample | mol characteristics | | | transition temp[a] (°C) | | | $T_{ODT}$ (°C) |
|---|---|---|---|---|---|---|---|
| | $f_{PEP}$ (vol %) | $M_n$ (kg/mol) | $M_w/M_n$ | $T_{\rightarrow HPL}$ | $T_{\rightarrow G}$ | $T_{\rightarrow HEX}$ | |
| PEP−PDMS-7 | 0.65 | 10.6 | 1.04 | | 122 | | 172 |
| PEP−PDMS-12 | 0.70 | 11.7 | 1.04 | | | | 174 |
| f69pd | 0.69 | | 1.04 | −8 | 41 | 83 | 175 |

[a] Heating at 1 °C/min.

are unusually long-lived nonequilibrium structures involved in the formation of the gyroid phase.[24] Most theoretical studies have found HPL structures to be unstable with respect to the LAM, HEX, or gyroid ordered phases (but with a free energy close to that of these stable phases).[11,12,25,26] However, Yeung et al. have accounted for a modulated lamellar structure allowing for composition fluctuations using a modified random-phase approximation.[27] Recent cell dynamics simulations of the time-dependent Ginzburg−Landau equation by Qi and Wang suggest that perforated and modulated layer structures may be metastable or transient structures, respectively, observed during a transition from the LAM to the HEX phases following a temperature jump.[28,29] Additionally, theoretical analysis of anisotropic composition fluctuations in the weak segregation limit[30] enables a description of observed SANS patterns[3,4,20] of the pseudostable perforated LAM structures, although these structures have not been unambiguously identified by scattering experiments. Also Laradji et al. have found the perforated layer structures to be unstable by means of a theory of anisotropic composition fluctuations.[31] Anisotropic composition fluctuations could be induced or amplified by strong shear or flow fields, but the mechanism for the interaction between such fields and composition fluctuations is not understood presently.

## Experimental Section

Diblock copolymers containing blocks of PEP and PDMS were synthesized by anionic polymerization of polyisoprene−poly(dimethylsiloxane) (PI−PDMS) diblock copolymers followed by catalytic deuteration of the PI blocks. This produced PEP−PDMS diblock copolymers having contrast for neutron as well as X-ray scattering. Details of the sample synthesis are described elsewhere.[13]

Two samples, PEP−PDMS-7 and PEP−PDMS-12, were synthesized to have PEP volume fractions $f_{PEP} = 0.65$ and $f_{PEP} = 0.70$, respectively. Stoichiometric data from the synthesis allowed us to calculate the volume fraction of $f_{PEP}$ and the overall number-average molar mass $M_n$ very accurately. After synthesis, these properties of the polymers were confirmed by independent measurements. The volume fraction was measured by NMR, and matrix-assisted laser desorption/ionization time-of-flight mass spectroscopy (MALDI-TOF-MS) measured the number-average molar mass $M_n$. A HP G2025A MALDI-TOF system was used for the verification of the molar mass. For this purpose, a matrix−silver solution in toluene was prepared by mixing a 0.1 M solution of dithranol (1,8,9-trihydroxyanthracene) and a 0.02 M solution of silver trifluoroacetate in a 10:1 ratio. The polymer sample was diluted to 5 mg/mL in toluene and mixed with the matrix−silver solution in a 1:10 ratio. A drop of this solution was placed on the HP sample holder and dried under vacuum prior to the MALDI-TOF measurement.

We blended a sample, f69pd, in the weight ratio 1:3 from the two neat diblock copolymer melts PEP−PDMS-7 and PEP−PDMS-12, respectively, resulting in an average volume fraction $f_{PEP} = 0.69$. The blend was prepared through codissolution in *n*-hexane followed by evaporation of the solvent. The molar mass distribution was provided by GPC that measured the polystyrene equivalent of the polydispersity index $M_w/M_n$. Properties of the three samples studied here are listed in Table 1 together with transition temperatures obtained from rheology measurements (see below). The glass transition temperatures for PEP[32] and PDMS[33] are $T_{g,PEP} = -56$ °C and $T_{g,PDMS} = -127$ °C, respectively.

Measurements of the dynamic shear moduli were made using a Rheometrics RSA II rheometer, using the shear sandwich configuration. The strain amplitude during rheological measurements was fixed at 1%, which is within the linear viscoelastic regime for these polymers. The reciprocating shear frequency was fixed at 1 rad/s. Samples were kept in a temperature-controlled nitrogen atmosphere for temperatures greater than 100 °C. The sample thickness between the sandwich shear plates was 2 × 0.3 mm.

SANS experiments were performed simultaneously with rheology measurements using a modified Rheometrics RSA II rheometer at the SANS instrument at Risø National Laboratory. Shear sandwich components machined from aluminum replaced the parts supplied with the rheometer to allow passage of the neutrons to the SANS detector. The absorption cross section of aluminum for neutrons is very small, which makes this material almost transparent to neutrons. A neutron wavelength $\lambda = 5.58$ Å$^{-1}$ was selected, with a spread $\Delta\lambda/\lambda = 0.09$, and the sample−detector distance was typically 3 m.

SAXS experiments were performed on beam line 8.2 of the Synchrotron Radiation Source (SRS) at the Daresbury Laboratory. Details of the storage ring, radiation, camera geometry, and data collection electronics have been given elsewhere.[34] A beam of $\lambda = 1.50 \pm 0.01$ Å X-rays was used, and the instrument was equipped with an area detector located 3 m from the sample position. The samples were sheared manually for the SAXS experiments in custom-made cells consisting of a piece of aluminum with machined side grooves to allow movement of a parallel aluminum slider during shear. Sample thickness was 0.5 mm. The beam passed through a hole of 3.0 mm in diameter. The inside of the cell was covered with Kapton tape. The polymers were sheared at ∼1 Hz for 50 cycles and 200% strain. The sample was heated via heat tape stuck on the cell, which gave relatively precise temperature control (±5 °C).

## Results and Discussion

**1. Scattering.** The structures of the ordered phases of PEP−PDMS-7 and PEP−PDMS-12 were determined using SAXS. To clarify further discussion, we first introduce the axis system for the shear geometry in Figure 1. The shear axis is along *x*, and the shear gradient direction lies along *y*. This is identical to the actual laboratory frame used for the manual shear alignment. However, the shear alignment performed on the rheometer was performed with the shear axis along the vertical. For the sake of comparison all two-dimensional scattering data will be shown with the shear axis along the horizontal as illustrated in Figure 1. SAXS patterns from the different phases observed rheologically (see below) with PEP−PDMS-7 are shown in Figure 2. Figure 2a shows two rings in the ratio 1:2 at 20 °C. The intensity of the inner ring is more than four times greater than the intensity of the outer ring.

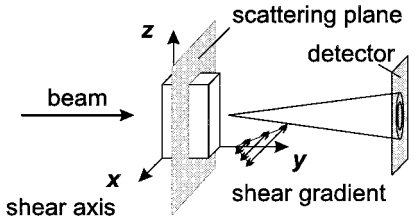


**Figure 1.** Definition of the axis system for the shear experiments, in this case related to the small-angle scattering experiment in the typical setting where the $x-z$ shear plane is oriented in parallel with the scattering plane. The shear axis is $x$, and the shear gradient is $y$.

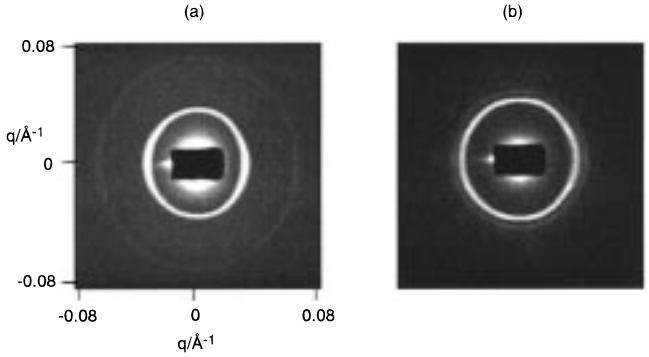


**Figure 2.** SAXS patterns of PEP−PDMS-7 identifying two ordered phases: (a) LAM at 20 °C with two rings of scattered intensity in the ratio 1:2. (b) Gyroid at 150 °C with two closely spaced rings in the ratio $6^{1/2}$:$8^{1/2}$.

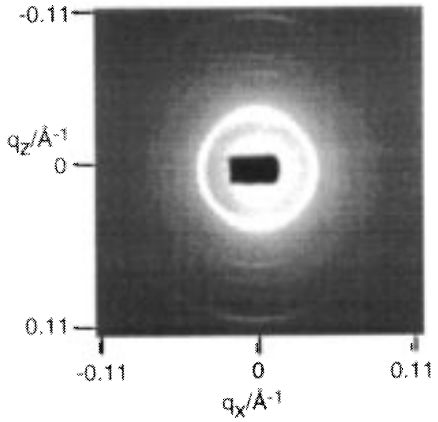


**Figure 3.** SAXS pattern at room temperature of PEP−PDMS-12 identifying it to be the HEX phase with reflections in the ratio 1:$3^{1/2}$:$4^{1/2}$:$7^{1/2}$.

At 150 °C in Figure 2b, two closely spaced rings are observed in the ratio $6^{1/2}$:$8^{1/2}$, consistent with the gyroid structure. This confirms the assignment of phases made earlier by SANS.[13]

Figure 3 shows a diffraction pattern obtained from PEP−PDMS-12 at room temperature, following shear. The presence of arced reflections in the positional ratio 1:$3^{1/2}$:$4^{1/2}$:$7^{1/2}$ indicates a HEX structure. Since the scattering is concentrated along the $q_z$ axis, the cylinders are primarily oriented in the shear direction, $x$. These data indicate that the single ordered phase revealed rheologically for PEP−PDMS-12 is a HEX phase.

**2. Rheology.** While it is not possible to determine an ordered structure unambiguously from dynamic mechanical spectroscopy, the order−order transitions (OOT) and the ODT can be precisely located, and the rheology trace of a temperature scan can be suggestive

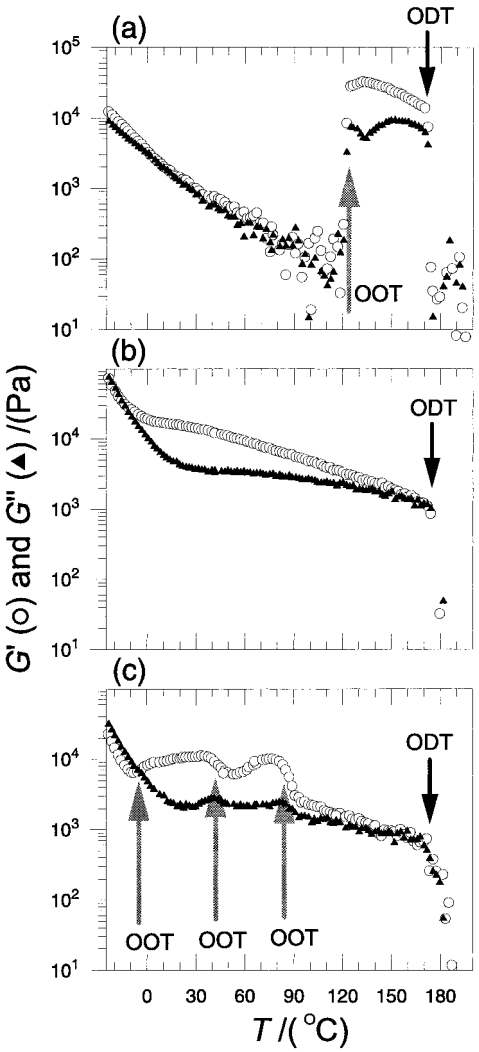


**Figure 4.** Temperature dependence of dynamic shear moduli. (a) PEP−PDMS-7 at shearing conditions $\omega = 1$ rad/s and $\gamma = 1\%$ and heating at 1 °C/min. (b) PEP−PDMS-12 at conditions $\omega = 1$ rad/s and $\gamma = 1\%$ and heating at 1 °C/min. (c) f69pd at conditions $\omega = 1$ rad/s and $\gamma = 1\%$ and heating at 0.5 °C/min.

of what phase or phases the sample exhibits. Figure 4a shows results from a temperature ramp of PEP−PDMS-7 heating at 1 °C/min. In agreement with earlier studies,[13] this sample has two ordered phases below the ODT at $T_{ODT} = 172$ °C. The low-temperature phase is LAM, and above the OOT (at this heating rate) 122 °C, the sample is in the G phase. The isochronal temperature ramp (1 °C/min) for PEP−PDMS-12 shown in Figure 4b indicates that above 0 °C, $G'$ and $G''$ decrease smoothly up to an ODT at $T_{ODT} = 174$ °C. Thus, this sample exhibits a single ordered phase, which according to the SAXS pattern shown in Figure 3, is HEX, in agreement with the composition.

Results in Figure 4c from rheology experiments with the mixed sample, f69pd, reveal the existence of multiple ordered phases. An isochronal temperature ramp, heating at 1 °C/min, shows a crossover of $G'$ and $G''$ and an increase in $G'$ at about $T_{OOT} = -8$ °C, which suggests an OOT from the low-temperature ordered phase to another ordered phase. At $T_{OOT} = 41$ °C, the slope of both shear moduli changes sharply, indicating a second OOT. At $T_{OOT} = 83$ °C, there is another point of inflection in both $G'$ and $G''$, indicating a third OOT. Finally, both moduli decrease dramatically at the order−disorder transition, at $T_{ODT} = 174$ °C. The

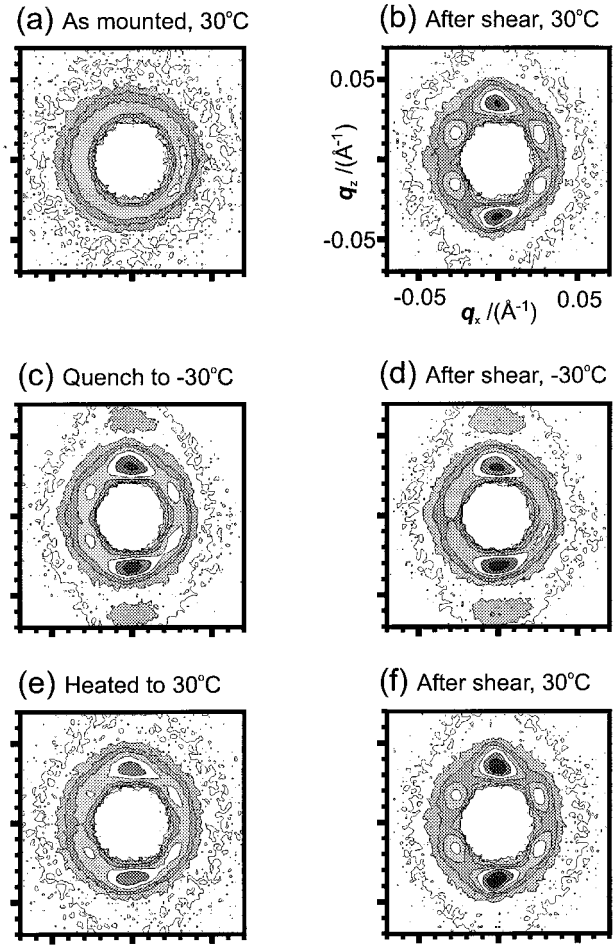


**Figure 5.** SANS data of a shear−cool cycle for f69pd that shows the reproduction of the HPL-like scattering pattern. (a) The scattering pattern from the sample after being mounted at 30 °C. (b) The pattern after shear at 30 °C. (c) The pattern following a quench to −30 °C. (d) After being sheared at −30 °C. (e) Following a temperature jump to 30 °C. (f) After being sheared at 30 °C the sample completes the cycle, and the pattern is similar to (b). The intensity is plotted on the same logarithmic scale for all SANS patterns mapped with three contour levels per decade.

identification of the ordered morphologies of f69pd is discussed below. Table 1 lists the transition temperatures together with molecular characteristics of the three samples.

**3. HPL Structure.** The Rheometrics RSA II rheometer installed at the SANS instrument at Risø gives the opportunity to make oriented samples by shear alignment, which changes the texture into a more single-crystal-like morphology of long-range order. When the sample is quenched into the ordered state at temperatures below the ODT, the ordered domain morphologies are typically distributed at random orientations. Scattering of such powderlike samples gives isotropic Debye−Scherrer rings of intensity. By applying large shear strains to the sample (∼100%), it is possible to align the macroscopically isotropic sample into long-range ordered macroscopic domains with anisotropic scattering patterns.

The stability of the HPL-like structure in the f69pd sample was systematically studied by use of shear and temperature cycles. The sample was mounted at room temperature (30 °C) for SANS experiments. The SANS scattering pattern as shown in Figure 5a reveals an isotropic ring typical for an unoriented sample. Shearing the sample at a frequency $\omega = 100$ rad/s and a shear strain amplitude $\gamma = 100\%$ introduced a more single-crystal-like orientation of the sample. The resulting scattering pattern shown in Figure 5b resembles that for the HPL structure previously found by Hamley et al.[20,21] The strong meridional reflections along the $z$ direction indicate that this phase is layered; the off-meridional reflections at 55 ± 5° with respect to the meridian characterize the stacking of in-layer perforations or composition variations. The pattern changed with time and was fully developed after two shearing cycles of 10-min duration each, interrupted by a 10-min cessation for relaxation. Following this, the sample was quenched to −30 °C. Two second-order spots (at $2q^*$) from the layered structure are observed along the $z$ direction (Figure 5c) while the six-spot pattern is still present. After 20 min of shearing at $\omega = 1$ rad/s and $\gamma = 100\%$ at −30 °C, the off-meridional spots disappear, and in Figure 5d, the scattering is typical for that of layers preferentially oriented in the perpendicular position[35] with the first- and second-order spots of scattering along $z$. Setting the sample temperature back to 30 °C (quiescently) causes the six-spot pattern to return as shown in Figure 5e. The weaker off-meridional reflections are fully restored in Figure 5f after a 10-min shearing cycle at $\omega = 100$ rad/s and $\gamma = 100\%$. We return to a more detailed discussion of the structure of this phase, elucidated via high-resolution SAXS experiments in section 8.

**4. Gyroid Phase Grown from HPL.** We were able to correlate in real time the rheological properties of multiple ordered phases in a diblock copolymer melt with its structure, by performing simultaneous rheology and SANS measurements. This gave us the opportunity to make correlated time-resolved studies of the kinetics as well as the epitaxy involved with the growth process from the HPL-like structure to the gyroid phase.

After the preparation described above, and illustrated in Figure 5, the temperature was set to 40 °C. Figure 6 shows SANS and rheology data for f69pd during the development of the gyroid phase at this temperature. The intensity scattered by the sample was collected into one 2D frame of SANS data. The rheology data was collected almost continuously (every 20 s) at conditions of minute shear strain ($\gamma = 1\%$) which is assumed not to affect the structural dynamical properties of the sample significantly. The time for collecting one SANS data frame is marked by gray bars in the rheology data in Figure 6. The dynamic elastic shear modulus is substantially larger than the dynamic loss shear modulus throughout this experiment, indicating that the ordered phases are solidlike. The diffraction pattern of the initial structure is shown in pattern 1. After 60 min, both $G'$ and $G''$ reach a minimum. The scattering (pattern 2) shows strong reflections from the layered structure while the off-meridional spots are very weak but still at an angle of 55 ± 5° with respect to the meridian. After 120 min (pattern 3), the off-meridional spots have moved to an angle of 70.5° with respect to the meridian. The meridional spots are ∼1 order of magnitude more intense than the off-meridional reflections, but beginning to broaden out. These changes are more clearly displayed after 180 min (pattern 4), where $G''$ reaches a maximum and $G'$ is rapidly increasing. The transition into the gyroid phase is now complete with the characteristic 10-spot pattern of the gyroid structure (see section 5), but $G'$ is still far from its final

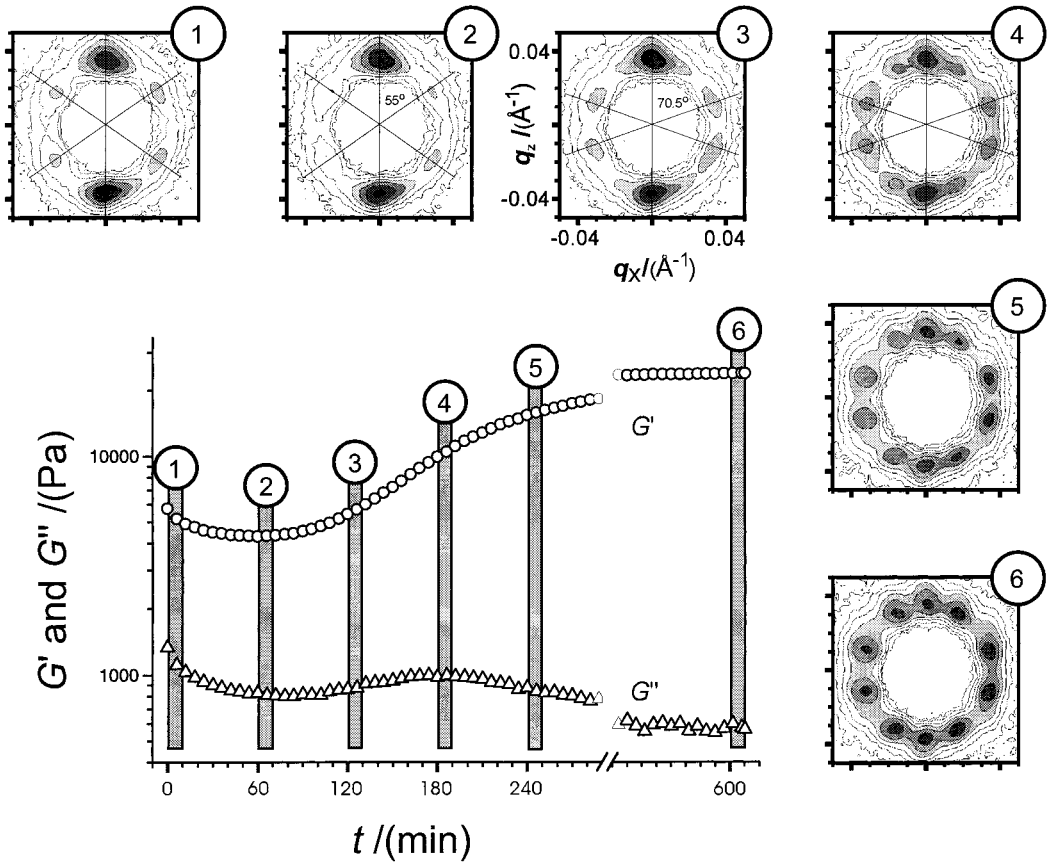


**Figure 6.** Changes in rheology and SANS data for f69pd during the isothermal growth of the gyroid phase from the HPL structure at constant temperature. The dynamic shear modulus were measured at $\omega = 1$ rad/s, $\gamma = 1\%$, and $T = 40$ °C. The intensity is plotted on the same logarithmic scale for all SANS patterns mapped with three contour levels per decade.

value. Only after 240 min, the dynamic shear moduli then begin to plateau (pattern 5), $G'$ increasing slightly and $G''$ decreasing slightly. The 10-spot SANS pattern sharpens up and is retained up to the end of the experiment after ~10 h (pattern 6), where all spots have approximately the same intensity.

Comparison of the SANS scattering pictures and the rheology trace in Figure 6 shows that the off-meridional reflections lose intensity and that the dynamic shear moduli drop slightly during the first 60 min (patterns 1 and 2). This indicates that the structure causing the HPL-like scattering deteriorates before the gyroid structure grows in. After 60 min, the changes in both scattering and rheology indicate the growth of the gyroid structure (patterns 3 and 4), as the 10-spot pattern develops and the value of $G'$ reaches orders of $10^4$ Pa. This experiment shows that the characteristic time for the formation of the gyroid phase from the HPL structure in this sample at this temperature is ~180 min. Because the strong meridional peaks from the layers in the HPL structure transform into the meridional peaks from the gyroid phase (⟨211⟩ reflections, see section 5) the data suggest an epitaxial relationship between the layers of the HPL structure and the {211} planes of the gyroid structure. There is no epitaxial relationship between the off-meridional peaks in the HPL-like and the gyroid patterns, because these peaks clearly shift position during the growth process, indicating that the off-meridional reflections are from different structures. It should finally be noted that the observation of growth of the gyroid phase at 40 °C proves that the HPL structure is not thermodynamically stable but rather a metastable phase or a long-lived dynamically accessed intermediate state between the LAM and gyroid phases. Hence, the OOT identified rheologically at −5 °C in Figure 4 is not an equilibrium phase transition but may represent the upper limit of stability of the LAM phase.

**5. Indexing of the Gyroid 10-Spot Scattering Pattern.** Diffraction patterns similar to those here (Figure 7, insets 4−6) have previously been identified as arising from various orientations of the $Ia\bar{3}d$ phase (associated with the gyroid structure) in lyotropic liquid crystals[8,36,37] and block copolymers.[1,3,4,38] A part of the reciprocal space of the $Ia\bar{3}d$ space group is shown in Figure 7a, displaying the first- and second-order reflections from the families of {211} and {220} reflection planes. The characteristic gyroid pattern of 10 first-order spots was previously indexed by Förster et al.[3] and Olsson and Mortensen,[39] who also attempted to rationalize the observation of 10 spots due to different projections of the reciprocal space. Extended studies[40] of the sample, f69pd, quenched to −100 °C from the fully developed and oriented gyroid phase show that the sample is aligned with the [111] lattice direction parallel to the shear direction $x$. However, the sample does not constitute a single-crystal domain, but it is a 2D powder made up of domains rotated randomly around the [111] lattice direction.[39] When neutrons are directed down the [111] direction (i.e., the scattering plane being the $y-z$ plane), the resulting scattering is accordingly an isotropic ring of intensity as observed experimentally.[40]

In SANS and SAXS experiments on polymer systems with large mosaic spread, the relevant part of the Ewald sphere can be approximated by a scattering plane

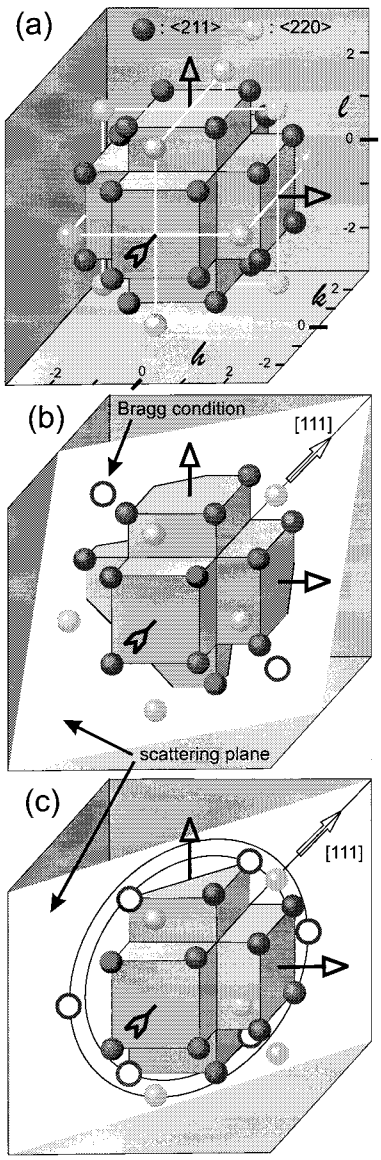


**Figure 7.** Reciprocal lattice of the gyroid structure of $Ia\bar{3}d$ symmetry. (a) The first two allowed reflections: ⟨211⟩ and ⟨220⟩, in a 3D projection. (b) A scattering plane oriented in the reciprocal space so that two ⟨220⟩ reflections meet the Bragg conditions. (c) A scattering plane oriented so that four ⟨211⟩ and two ⟨220⟩ reflections meet the Bragg conditions.

perpendicular to the incident beam, because the typical lengths of the scattering wave vectors are orders of magnitude smaller that the wave vector of the incident and elastically scattered radiation. Figure 7b shows the scattering plane intercepting the reciprocal lattice points $[\bar{2}02]$ and $[20\bar{2}]$. A single crystal of $Ia\bar{3}d$ symmetry oriented like this with respect to the scattering plane would give these two Bragg reflections in the same pattern, due to the finite collimation of the beam and out-of-plane mosaicity of the crystal structure. Rotating the scattering plane 30° around the [111] lattice direction, we get the orientation depicted in Figure 7c, where two sets of {211} planes and one set of {220} planes meet the Bragg conditions giving all together six spots of reflected intensity, two spots from each set of planes.

All possible scattering patterns, from individual single-crystal domains rotated randomly around the [111] direction, are shown in Figure 8a. The first pattern (a-I) corresponds to the single-crystal orientation with respect to the scattering plane, as shown in Figure 7b. The rotation angle, $\theta$, is assigned to be zero at this orientation, and the value of $\theta$ is given below the scattering pattern from each single-crystal domain. The orientation of the single-crystal domain with respect to the scattering plane, as illustrated in Figure 7c, corresponds to the pattern shown in Figure 8a-III. A full rotation (360°) of the reciprocal lattice, corresponding to the 2D powder, runs 3 times through this sequence of eight patterns. The patterns in Figure 8 correspond to planar cuts through the reciprocal lattice which can be related to crystal planes in the real space structure which are parallel to the $x-z$ shear plane in the coordinate system defined in Figure 1.

In Figure 8b and c, the indexing from above is compared to real data. We note that the ⟨211⟩ and ⟨220⟩ reflections in the SANS patterns are not very well resolved compared to SAXS data, which have better resolution clearly separating the first- and second-order reflections (see Figure 11c). The two concentric circles have the ratio $6^{1/2}$:$8^{1/2}$. Scattering from single-crystal domains with {220} crystal planes in parallel to the $x-z$ shear plane is mapped on top of the real data in Figure 8b. This corresponds to the scattering patterns illustrated in Figure 8a-III and -VII, which are of the same symmetry. The scattering from, for example, the orientation illustrated in a-VII gives a pair of meridional ⟨211⟩ reflections (at ±90°) and another pair of ⟨211⟩ reflections at −19.5 and 160.5° with respect to the [111] equator (identical to the shear direction $x$). At 35.3° and −144.7°, a pair of ⟨220⟩ reflections are present, belonging to the same domain. Twinning these two domains (Figure 8a-III and -VII) gives a six-spot pattern of first-order reflections. A scattering pattern like this from a polystyrene−poly(2-vinylpyridine) diblock copolymer mixture was identified and indexed by Schulz et al.[1]

Scattering from single-crystal domains with {211} and {321} crystal planes in parallel to the $x-z$ shear plane is mapped on top of the real data in Figure 8c. Here the patterns from Figure 8a−I and -V map onto the meridional ⟨220⟩ reflections. The patterns in Figure 8a-II and -IV give the ⟨211⟩ reflections at −61.87 and 118.13° from the equator, while the patterns in Figure 8a-VI and -VIII give the ⟨211⟩ reflections at −118.13 and 61.87° from the equator. A scattering pattern from a polyisoprene−polystyrene diblock copolymer melt dominated by scattering from domains with {321} crystal planes in parallel with the shear plane and oriented with respect to the [111] direction as shown in Figure 8c was observed by Khandpur et al.[4]

**6. Gyroid Phase Grown from Quenched HEX Phase.** The kinetics and the epitaxy of growth of the gyroid phase at 60 °C following a quench from the high-temperature HEX phase at 120 °C was investigated using simultaneous SANS and rheology measurements as illustrated in Figure 9. Prior to this experiment the sample, f69pd, was heated at 10 °C/min from 30 to 120 °C. At 120 °C it was left to equilibrate for ∼5 min and then quenched to 80 °C where the cooled HEX phase was subjected to $\omega = 100$ rad/s and $\gamma = 100\%$ for 20 min, after which the scattering showed strong, slightly arced meridional reflections at $q^*$ superimposed on a ring of scattering, with a weak higher-order reflection at $3^{1/2}q^*$ (not shown in figure). This is characteristic of a HEX phase oriented with the cylinders parallel to the shear axis.[41−44] After the sample was cooled by 5 °C/min to 60 °C, the data shown in Figure 9 were collected, keeping the temperature constant at 60 °C. Each of the

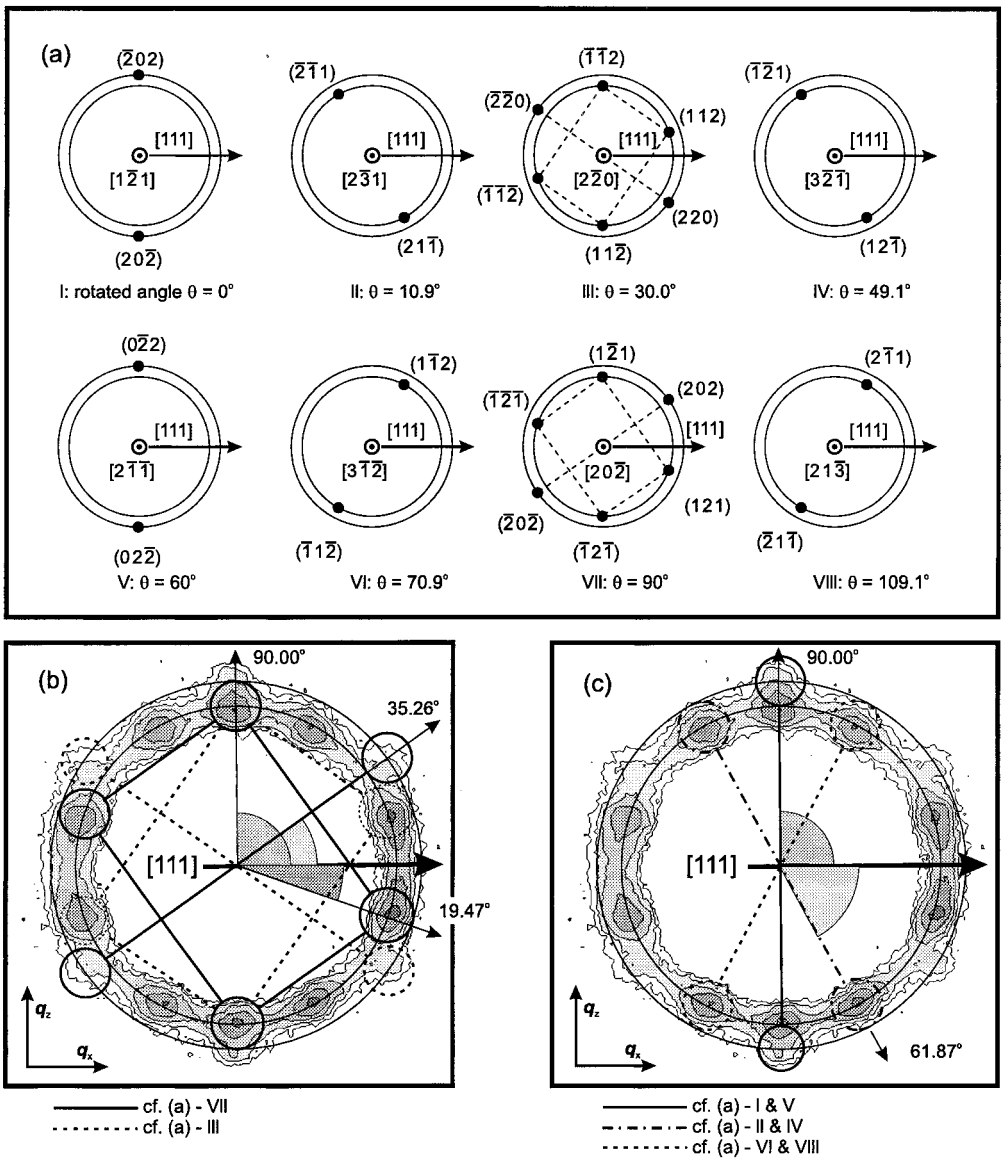


**Figure 8.** Diffraction patterns expected for single crystals of the $Ia\bar{3}d$ phase. (a) Sequence of eight diffraction patterns encountered as the gyroid structure is rotated round the [111] direction. Each pattern corresponds to a planar cut through the reciprocal space. The normals to the scattering planes are given, by the arrow pointing out of the paper. (b) The typical "10-spot" gyroid diffraction pattern compared to expected patterns from orientations where {220} crystal planes are in parallel with the scattering plane. (c) The "10-spot" pattern compared to expected patterns from orientations where {211} and {321} crystal planes are in parallel with the scattering plane.

SANS patterns in Figure 9 shows the integrated intensity over a period of 10 min which is illustrated by the width of the bars, as in Figure 6. Initially, the SANS pattern 1 was obtained, corresponding to the state where $G'$ and $G''$ are both quite low. The dynamic shear moduli then begin to increase rapidly until $G''$ reaches a maximum after ~60 min (between patterns 2 and 3) and a transformation to the gyroid phase, characterized by the 10-spot diffraction pattern, has occurred after 90 min (pattern 3). The rate of change of $G'$ then decreases as the ordering of the gyroid structure is perfected toward the end of the experiment after 12 h (patterns 4−6). The slight asymmetry of pattern 6 is due to an artifact related to variation in detector resolution. Because this pattern grew from that of the HEX phase without application of large-amplitude shear, and because the meridional reflections remain in the same position throughout the transition, these data show an epitaxial relationship between the two structures. The orientation of the initial phase is that of HEX-packed cylinders aligned in the shear direction $x$. At least some fraction of the {11} planes is preferentially oriented in parallel with both the shearing and scattering planes. This would leave the {10} planes in Bragg position, as observed. In this orientation, the rods viewed edge-on along the direction of the incoming neutrons are in {10} planes, hence the first-order meridional ⟨10⟩ reflections (Figure 9, pattern 1). The gyroid 10-spot pattern retains this orientation and when fully developed after 12 h the meridional ⟨211⟩ reflections (see Figure 8a) are in the same position at the same $q$ value. This indicates that the spacing between {10} planes in the HEX phase matches the spacing between the {211} planes in the gyroid phase. This supports the epitaxial relationship between the hexagonal {10} planes and the gyroid {211} planes. This epitaxy is the same as that previously observed for the transition between HEX and gyroid phases in lyotropic systems[8,45] and another diblock copolymer system.[1,19]

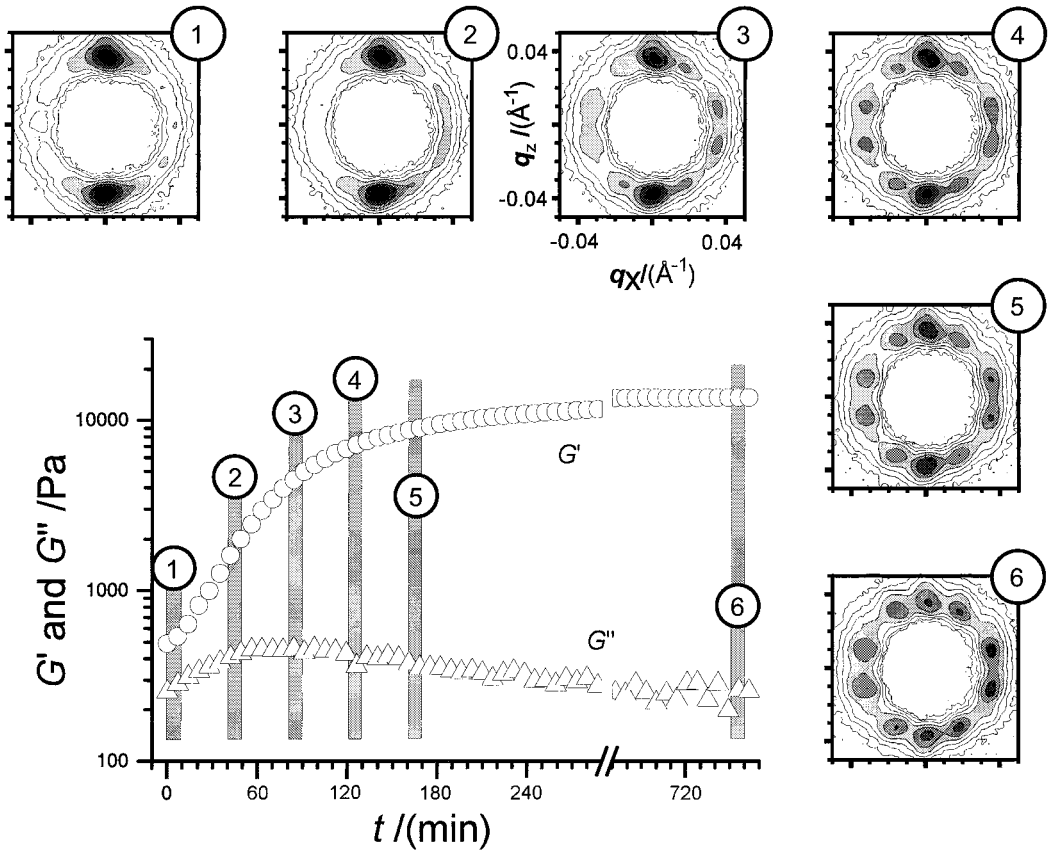


**Figure 9.** Changes in rheology and SANS data for f69pd during the isothermal growth of the gyroid phase from the HEX phase. Following a quench from 120 to 80 °C the sample was prepared for 20 min by $\gamma = 100\%$ and $\omega = 100$ rad/s. Then the temperature was set to 60 °C and the experiment started. The dynamic shear moduli were measured at $\omega = 1$ rad/s and $\gamma = 1\%$. The intensity is plotted on the same logarithmic scale for all SANS patterns mapped with three contour levels per decade.

From comparison of the SANS scattering pictures and the rheology trace a two-stage mechanism for the formation of the gyroid phase is indicated. During the first stage (patterns 1 and 2), the mechanical response from the sample changes most rapidly while the SANS picture does not give any recognizable scattering from the gyroid structure. The typical 10-spot gyroid scattering picture, however only weakly profiled, appears very suddenly in pattern 3, and the characteristic time for formation of the gyroid phase following this quench is from SANS estimated to be of the order of 90 min. During the first part of the transformation, where $G'$ increases rapidly, the mechanism suggested is one of formation of the complex gyroid structure, but without long-range orientational order for the structure; i.e., no Bragg peaks have appeared. This primary formation mechanism involves long time-scale dynamic processes that have not yet been elucidated. After 90 min (pattern 3 onwards), the shear moduli asymptotically tend to approach a final value. Subsequently the secondary mechanism, perfection of the ordered structures, is essentially complete after ∼180 min (pattern 5), although $G'$ continues to increase slightly after this. A two-stage mechanism for the developments of the LAM phase in a diblock copolymer following a quench from the disordered phase was observed by Stühn et al.[46] They suggested that the initial stage corresponds to formation of microphase-separated domains and the second to ordering of these domains onto a lattice. This process is analogous to that proposed by us for the transformation between ordered HEX and gyroid phases; however, the time scales are very different. Stühn et al. found that kinetic processes were completed within 100 s[46] whereas the time scale for formation of the gyroid phase in our polymer is several hours.

**7. Gyroid Phase Bypassed: Cooling from HEX to HPL.** After having examined the stability of the sample, f69pd, at 40 and 60 °C, we turned to study the reversibility of the transitions shown in the rheology trace in Figure 4c with respect to temperature. The formation of ordered phases during a slow cool from a shear-aligned HEX phase was found to be quite distinct from that observed following a fast quench. Figure 10 presents simultaneous SANS and rheology data acquired during slow cooling (0.4 °C/min to 0 °C and then 2 °C/min) from the HEX phase, starting at 80 °C. Prior to this experiment, the sample was shear-aligned at 120 °C by applying $\omega = 100$ rad/s and $\gamma = 100\%$ for 10 min. The SANS pictures show the scattered intensity integrated over 5 min. Confirmation of the initial HEX structure is provided by the SANS pattern 1, which is characteristic of a HEX phase with a strong first-order reflection and a hint of the second-order reflection at $3^{1/2}q^*$ from the cylinders aligned along the shear axis (see Figure 9 and discussion above). The sample in the HEX phase supercools down below 40 °C (pattern 2). At 35 °C, both $G'$ and $G''$ increase rapidly, indicating an OOT. The diffraction patterns corresponding to temperatures between 25 and −10 °C (patterns 3 and 4) resemble the HPL-like patterns shown in Figures 5 and 6. In particular, strong meridional reflections with higher orders at $2q^*$ and off-axis reflections at $55 \pm 5°$ with respect to the meridian are observed. This phase can be cooled to −18 °C, at which point $G''$ becomes larger than $G'$, and the off-meridional peaks start losing intensity. The ordered phase was cooled to −50 °C, and

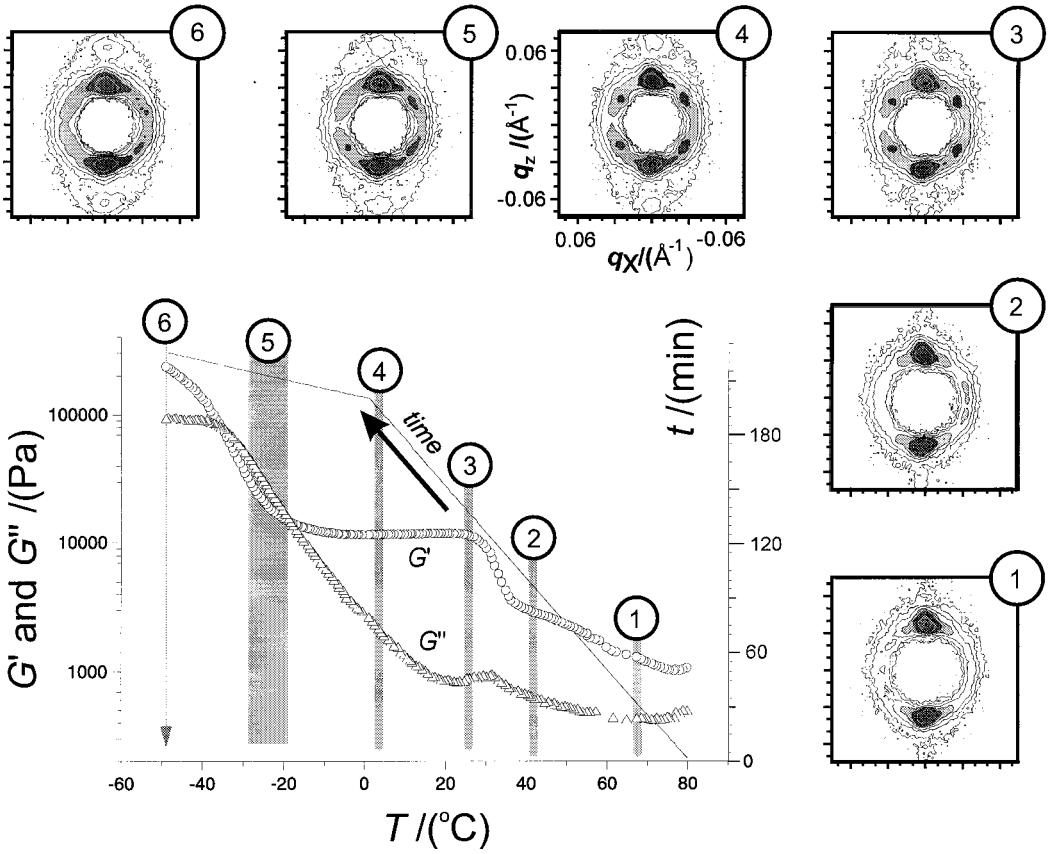


**Figure 10.** Changes in rheology and SANS data for f69pd cooling from the HEX phase at 80 °C. The dynamic shear moduli were measured at $\omega = 1$ rad/s, $\gamma = 1\%$, and a cooling rate of 0.4 °C/min to 0 °C and then 2 °C/min. Prior to this slow cool, the sample was shear aligned at 120 °C by applying $\omega = 100$ rad/s and $\gamma = 100\%$ for 10 min. The intensity is plotted on the same logarithmic scale for all SANS patterns mapped with three contour levels per decade.

after 5 min of equilibration, the SANS pattern (pattern 6) showed a typical signal from a layered structure with meridional reflections at $q^*$ and $2q^*$ as observed in Figure 5d. The dynamic shear moduli are difficult to interpret at these temperatures due to the proximity of $T_g$ for the PEP block.

If we define the start of the transformation to the HPL-like structure at 40 °C, then the sample transforms to HPL (completion at 25 °C) in ~38 min and stays in this state for a further ~100 min until the scattering pattern 6 indicates a LAM structure. This is significant because both the times for transformation and the total time in the HPL-like structure are smaller than the time scale for even the primary growth process of the gyroid phase indicated by Figure 6, where the sample is held at 40 °C in the HPL-like state and the estimated time for growth of the gyroid phase was 180 min. This suggests that following this path through temperature-phase space, the gyroid phase does not have time to grow, whereas transformation to the HPL structure occurs faster, and so this is observed as a transient or metastable structure instead.

During the experiment shown in Figure 10, the first-order meridional peaks in the HEX-phase transform into reflections from the planes in the layered HPL structure and the LAM phase, thus indicating an epitaxial relationship between the {10} planes in the HEX phase and the layers in the HPL structure.

**8. High-Resolution Studies of Ordered Phases.** In order to obtain better information on the structure of the ordered phases (especially HPL) of the f69pd sample, high-resolution X-ray scattering was performed at the Daresbury synchrotron. Because of the wavelength spread, SANS experiments cannot resolve closely spaced peaks and it is of limited resolution in comparison to SAXS. Reciprocating manual shear was used to orient the ordered phases observed in f69pd, which were examined using SAXS. These data are summarized in Figures 11 and 12 and are supported by recent experiments using a Rheometrics RSA II rheometer,[47] where the shearing conditions can be carefully controlled and simultaneously rheology and SAXS data acquired.

Figure 11 shows the effect of shear on the sample as mounted at room temperature, which was unoriented and produced a single diffraction ring (Figure 11a). Following manual shear ($\omega = 1$ Hz, $\gamma \sim 200\%$ for 50 cycles), the pattern in Figure 11b was obtained. This shows a highly anisotropic scattering pattern which can be described by separating the peaks into three groups: (1) strong meridional reflections are present with a broad inner doublet and higher-order meridional reflections which is in the positional ratio 1:2 with respect to the strongest reflection (of larger $q$) of the inner doublet. (2) The six innermost diffraction peaks (at $q^*$) are arranged hexagonally with two meridional reflections (the weaker reflections of the inner doublet) and four off-meridional reflections. Higher-order reflections from the hexagonal structure are located at $3^{1/2}q^*$ on the upper and lower parts of the pattern. (3) Finally, a set of reflections located at $(3/2)^{1/2}q^*$ is arranged as a square with sides parallel to the vertical and horizontal axis.

The presence of the square arrangement of higher-order reflections is very unlikely to be due to a super-

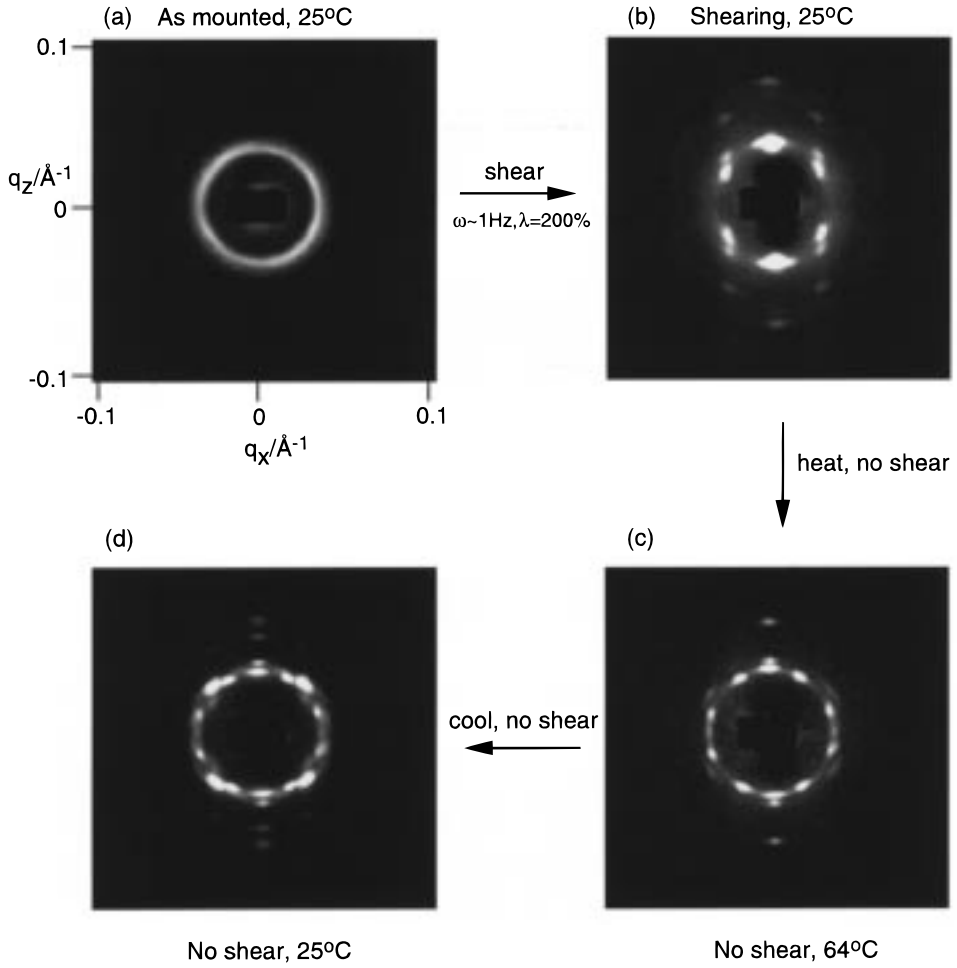


**Figure 11.** SAXS patterns for f69pd recorded during a shear−heat−cool cycle. The sample was manually sheared ($\gamma \sim 200\%$ and $\omega \sim 1$ Hz) for ~1 min in a custom-made shear cell. (a) Sample as mounted. (b) Shear-oriented HPL structure. (c) Oriented gyroid phase. (d) Cooled from the gyroid phase.

position of two-spot patterns from HEX and LAM phases at right angles. Furthermore, the splitting of the inner meridional layer peak is not due to the gyroid phase, so this phase cannot be a coexistence of monodomains of any of the LAM, HEX, or gyroid phases. This pattern instead appears to be a high-resolution version of the diffraction pattern of the HPL structure observed previously using SANS and discussed here in the context of Figures 5, 6, and 10.[20,21] Apparently neither the meridional doublet nor the off-meridional pairs of peaks could be resolved by SANS. In the next section, we return to a discussion of possible morphologies that could cause these HPL-like scattering patterns. On heating to 64 °C, without shear, the HPL diffraction pattern transforms into that characteristic of a well-oriented gyroid phase, as shown in Figure 11c. This transformation appears to occur epitaxially, as suggested by the retention of the position of the meridional reflections. The 10-spot pattern of ⟨211⟩ reflections and 6-spot pattern of ⟨220⟩ reflections is discussed above (see Figures 7 and 8 for indexation). There is also a pair of higher-order reflections at $(^{16}/_{6})^{1/2}q^*$ from planes aligned parallel to the axis along which the sample was previously sheared. This is an allowed reflection for the $Ia\bar{3}d$ phase, for which the magnitudes of $(h^2 + k^2 + l^2)$ for allowed ⟨$hkl$⟩ reflection are shown in Table 2. Upon cooling, the symmetry of the diffraction pattern from the gyroid phase is spontaneously broken, without the application of shear, and the SAXS pattern shown in

**Table 2. First 20 Allowed Reflections for the $Ia\bar{3}d$ Phase**

| $hkl$ | $(h^2 + k^2 + l^2)$ | $hkl$ | $(h^2 + k^2 + l^2)$ |
|---|---|---|---|
| 211 | 6 | 611/532 | 38 |
| 220 | 8 | 620 | 40 |
| 321 | 14 | 541 | 42 |
| 400 | 16 | 631 | 46 |
| 420 | 20 | 444 | 48 |
| 332 | 22 | 543 | 50 |
| 422 | 24 | 640 | 52 |
| 431 | 26 | 721/552 | 54 |
| 521 | 30 | 642 | 56 |
| 440 | 32 | 732/651 | 62 |

Figure 11d is obtained at room temperature, after 10-min equilibration. The square of reflections characteristic of the HPL pattern in Figure 11b have returned and coexists with residual peaks from the gyroid phase. Higher-order reflections from the gyroid phase are observed along the meridian at $(^{16}/_{6})^{1/2}q^*$ and $(^{20}/_{6})^{1/2}q^*$. This SAXS pattern indicates that the gyroid structure does not supercool as a single phase, but that (partial) transformation to the HPL phase occurs spontaneously on cooling. This is a surprising result as the dynamical elastic shear modulus $G'$ of this sample (not illustrated)—and a selection of other diblock copolymers[24]—show no indication of a partial transformation to the HPL structure when cooling from the gyroid phase.

SAXS data obtained during a second shear−heat cycle are presented in Figure 12. The initial state is that shown in Figure 11d, i.e., a gyroid phase partially

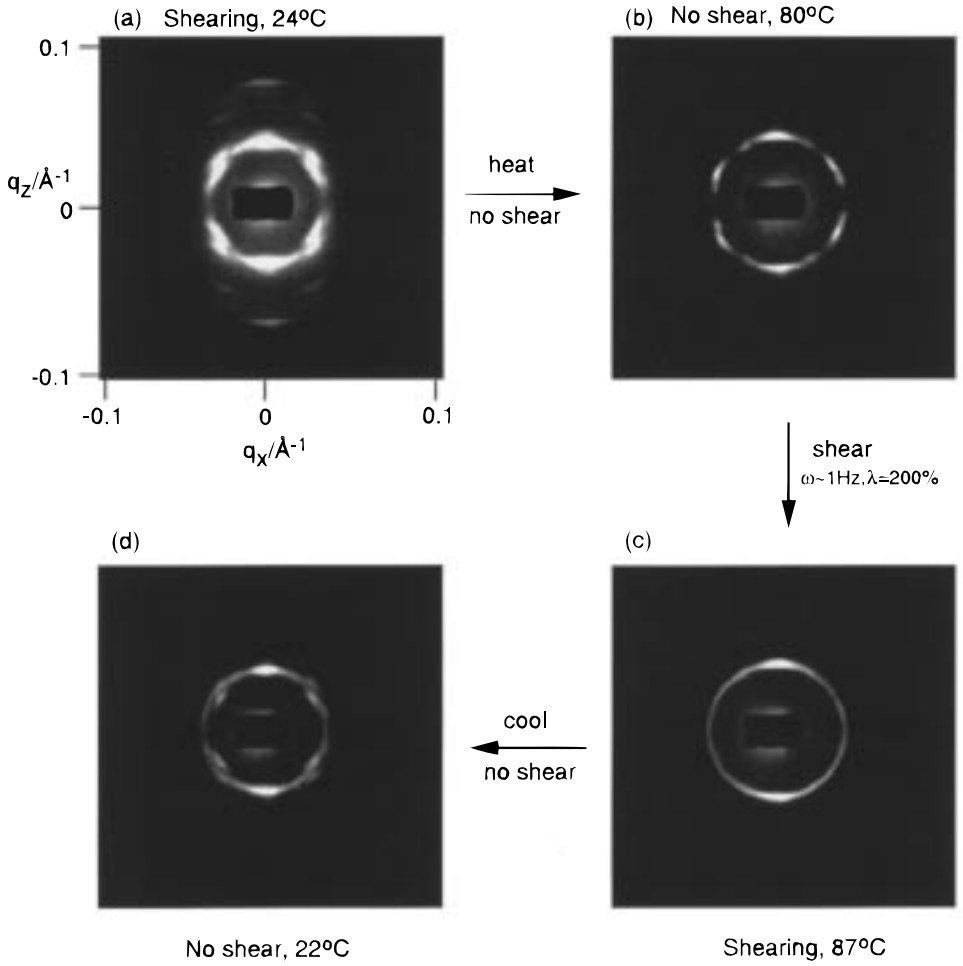


**Figure 12.** SAXS patterns for f69pd during a second shear−heat−cool cycle. The sample was manually sheared ($\gamma \sim 200\%$ and $\omega \sim 1$ Hz) for ~1 min in a custom-made shear cell. (a) Shear-oriented HPL phase (from Figure 11d). (b) Gyroid phase at the brink of transforming to the HEX phase. (c) Shear-oriented HEX phase. (d) HPL structure reproduces by quiescent cooling from the HEX phase.

transformed to the HPL structure. Shearing at room temperature produces the pattern shown in Figure 12a, which is similar to Figure 11b, and indicates that an oriented HPL structure has been sheared in. The gray levels in Figure 12a have been adjusted to highlight the higher-order reflections, the meridional reflections actually being ~1 order of magnitude more intense than the first-order off-meridional peaks, consistent with a layered structure. On slow heating (~3 °C/min) to 80 ± 5 °C, transformation to a gyroid phase occurs, as revealed by the SAXS pattern in Figure 12b. This pattern is similar to the one of an oriented gyroid phase shown in Figure 11c. However, it does not show sharp reflections, which could be because the sample is just below its order−order transition temperature at 80 °C (see Figure 4c). On shearing at 87 ± 5 °C, the sample passes the order−order transition and the pattern in Figure 12c results. The scattering shows a ring with sharp reflections superimposed on the meridian. This can be identified as arising from the HEX phase with the rods oriented along the shear direction *x*, supported by the presence of higher-order reflections at $3^{1/2}q^*$ (not shown).[41−44] Rapid quenching to 22 ± 5 °C of the high-temperature HEX phase leads to the spontaneous reappearance of the HPL phase shown in Figure 12d, confirming the results of the slow-cool experiment shown in Figure 10. The orientation matches the one previously accessed (Figure 11b).

Following this, the sample was removed from the X-ray beam line in the shear cell and stored at room temperature for three months. After this time, the sample was remounted, and a diffraction pattern consisting of a polydomain pattern of largely isotropic scattering data was obtained. This was reduced to a one-dimensional form, and the resulting profile is shown in Figure 13. The indexation in this pattern (see Table 2) shows that the structure is of *Ia*3*d* symmetry, and thus the HPL phase eventually relaxes to the gyroid phase. This strongly suggests that the HPL is a long-lived metastable phase or intermediate state and not an equilibrium phase, in agreement with other studies.[24] As shown in Figure 6 at 40 °C, the HPL to gyroid transition occurs in ~3 h, and further work is in progress to determine the lifetime of this phase under other preparation conditions such as those corresponding to Figures 11 and 12.

**9. Modeling of the HPL Structure.** Theoretical work by Qi and Wang[30] suggests that the morphology of the metastable HPL structure is caused by unstable density fluctuations in the LAM phase. An ABAB... stacking sequence of layers in the HPL state is anticipated as the amplitude of the anisotropic fluctuations diverge when the LAM phase reaches its spinodal upon heating. The metastable structure that forms upon transition to the HPL state is indeed a physical structure of a characteristic density profile that exhibits

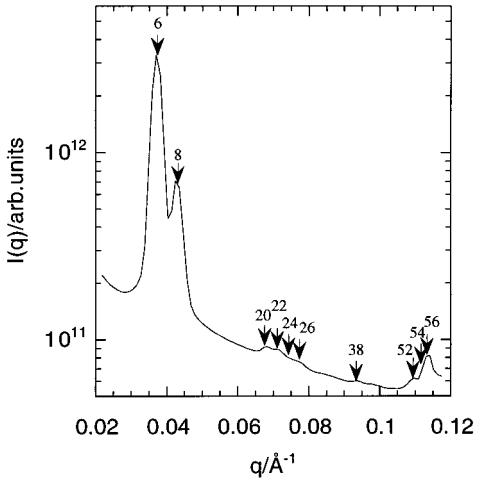


**Figure 13.** SAXS profile (at room temperature) of sample initially in the HPL phase (Figure 12d) retained in shear cell, after three months.

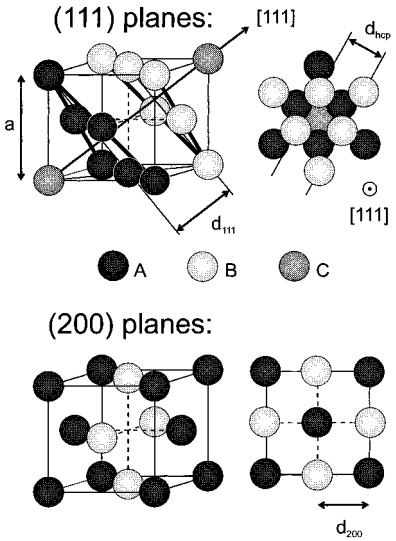


**Figure 14.** Principal planes giving rise to diffraction in an fcc structure.

Bragg reflections of first and higher orders as evidenced by the scattering patterns. The higher orders present in the HPL pattern (e.g., Figure 11b) illustrate the long-range single-crystal-like orientation of the sample.

The HPL structure can formally be modeled as stacked layers containing close-packed hexagonal perforations. In particular, the SAXS data can be described as resulting from a combination of ABCABC... and ABAB... packing of close-packed planes, i.e., as a combination of a face-centered cubic (fcc) structure and a hexagonal close-packed (hcp) structure. A similar model has been proposed for high-resolution SAXS patterns, resembling those for the HPL state presented here, by Diat and co-workers[48] following work by McConnell et al.[49] This is consistent with the fact that the critical packing fraction (in this case of perforations in the layers), 0.74, is the same for the fcc and hcp phases and the observation that these two structures may be nearly degenerate in free energy.[12,50] Figure 14 shows the unit cell of an fcc structure and the projections of the (111) and (200) planes. The *d*-spacings of the (111) and (200) layers are respectively $d_{111} = {}^1/_{3^{1/2}}a$ and $d_{200} = {}^1/_2 a$, where $a$ is the lattice spacing. Diffraction from the (200) planes gives rise to the four azimuthal maximums evident in the outer diffraction ring for the HPL pattern (e.g., Figure 11b). We note that scattering from an ABAB... stacking (see Figure 14, white and black spheres only) viewed along the [111] will give a hexagon of (in-layer) scattering, as seen in Figure 11b. The *d*-spacing related to this in-layer scattering is $d_{10} = ({}^6/_{16})^{1/2}$. The *d*-spacings listed here ($d_{111}$ and $d_{200}$ in the fcc structure and $d_{10}$ in the hcp structure) are related to wave vectors for the Bragg reflection from the (111) and (200) fcc planes ($q_{111}$ and $q_{200}$), and the in-layer hexagonal hexagonal hcp planes ($q_{10}$). Relative ratios with respect to the shortest wave vector are

$$\frac{q_{111}}{q_{10}} = \frac{d_{10}}{d_{111}} = \sqrt{\frac{9}{8}} \simeq 1.06 \quad (1)$$

$$\frac{q_{200}}{q_{111}} = \frac{d_{111}}{d_{200}} = \sqrt{\frac{4}{3}} \simeq 1.15 \quad (2)$$

$$\frac{q_{200}}{q_{10}} = \frac{d_{10}}{d_{200}} = \sqrt{\frac{3}{2}} \simeq 1.22 \quad (3)$$

The scattering picture in Figure 11b arises from grains corresponding to at least two orientations of the fcc–hcp model structure. In the [111] projection, with the (111) hcp planes aligned in parallel with the scattering plane, we have the inner hexagon of reflections $q^* = q_{10}$ (two meridional and four off-meridional spots) and four second-order off-meridional reflections at $q^* = 3^{1/2}q_{10}$. The four azimuthally equally spaced spots on the outer ring at $q^* = q_{200} = ({}^3/_2)^{1/2}q_{10}$ are due to scattering from (200) fcc planes and therefore are identical with a [100] projection. We speculate that the stronger meridional reflection of the inner doublet (the outer spot) and its second order at twice the $q$-value are due to scattering from (111) fcc planes aligned in the "perpendicular" orientation; hence the scattering at $q^* = q_{111} = ({}^9/_8)^{1/2}q_{10}$, and $2q^*$.

That a hexagon of reflections can result from a combination of hcp and fcc packing has been suggested previously by McConnell et al., who performed SANS on cubic micellar phases in block copolymer gels.[49] The result is a broadening of the fcc Bragg diffraction spots to Bragg rods. The resulting scattering from a combination of ABAB and ABCABC stacking is illustrated in reciprocal space as depicted in Figure 15. The intersection of the Bragg rods with the (111) plane, containing $q = 0$, produces the hexagonally arranged scattering maximums observed in the diffraction plane. Because the ⟨111⟩ reciprocal lattice points are not in the (111) scattering plane but either $\sin^{-1}({}^1/_3) = 19.47°$ above or below it as seen from the origin, we get the magnitude for the wave vector of the inner hexagon of reflections to be $\cos(19.47°) \times q_{111} = ({}^8/_9)^{1/2}q_{111} = q_{10}$ (cf. eq 1). Note that the wave vector magnitude and azimuthal position of the six hexagonal spots due to the Bragg rods are identical to the hexagonal in-layer reflections from the ABAB... stacking mentioned above. The ratios of the wave vectors derived from the real space *d*-spacings (Figure 14) are confirmed by looking at the reciprocal lattice structure (Figure 15).

## Summary

The rheological properties of a polymer sample are related with its structure—in real time. Simultaneous small-angle neutron scattering measurements and in

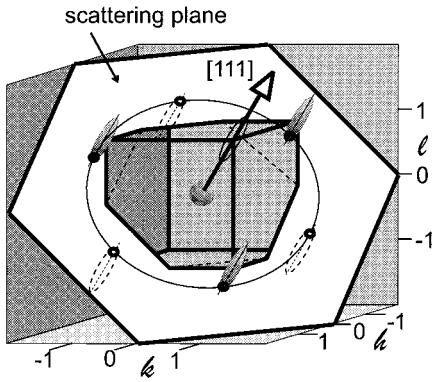


**Figure 15.** Reciprocal space of an fcc structure. Viewed along the [111] direction, none of the ⟨111⟩ reciprocal lattice points meet the Bragg conditions. If the ABCABC stacking sequence of (111) planes in the fcc structure is perturbed (for example, if there are hcp sequences of ABAB... stacking), the Bragg reflections are smeared into Bragg rods, as indicated. Then, a hexagon of spots is obtained in the scattering plane, containing $q = 0$, as shown.

situ rheology measurements was used to relate the macroscopic dynamical mechanical response and the mesoscopic structural behavior of a multiple ordered sample of poly(ethylene-*alt*-propylene)−poly(dimethylsiloxane) diblock copolymer. These studies show that the HPL phase is metastable, and for this particular sample, the HPL structure relaxes into the more stable gyroid phase, in agreement with theory. The study of a supercooled hexagonal phase relaxing to the gyroid phase confirmed previous findings for the epitaxial relationships between the hexagonal and gyroid phases. However, the transformation to the gyroid phase happens on a time scale of hours, which compared to typical experimental temperature ramps is rather slow. This means that the gyroid phase can easily be bypassed when the sample is heated or cooled too fast. The gyroid phase showed a typical 10-spot pattern when it was grown in oriented samples of the higher temperature hexagonal phase or the lower temperature HPL. This pattern was indexed following a scheme which suggests that the phase is a 2D powder of directionally oriented domains with the [111] crystal direction in parallel to the previously applied shear, but otherwise randomly rotated round this axis. Finally, high-resolution studies using synchrotron small-angle X-ray scattering was used to elucidate the structures of the various morphologies. These studies showed that that the gyroid structure does not supercool as a single phase, but reflections characteristic of the HPL structure appear when the sample is cooled. Puzzling SAXS patterns were obtained from the HPL-like structure, which may be modeled as a combination of stacking sequences of hexagonally perforated layers. In the Appendix, the morphology of the gyroid phase is discussed, and various real space projections of the structure are related to their resulting scattering patterns.

**Acknowledgment.** The authors are grateful to Mrs. L. Hansen and Dr. S. Ndoni for help with sample characterization, Dr. P. Sommer-Larsen for help with computer graphics, Dr. B. U. Komanschek for help with the X-ray experiments, and Dr. A. Likhtman and Prof. F. S. Bates for useful discussions concerning the gyroid structure. We are grateful to the materials SESS (U.K.) for the allocation of beam time, and I.W.H. and A.J.R. thank the EPSRC (U.K.) for support (Grant GR/K05982) that funded J.P.A.F.. This research was supported by the Danish Polymer Center at Risø National Laboratory (Denmark).

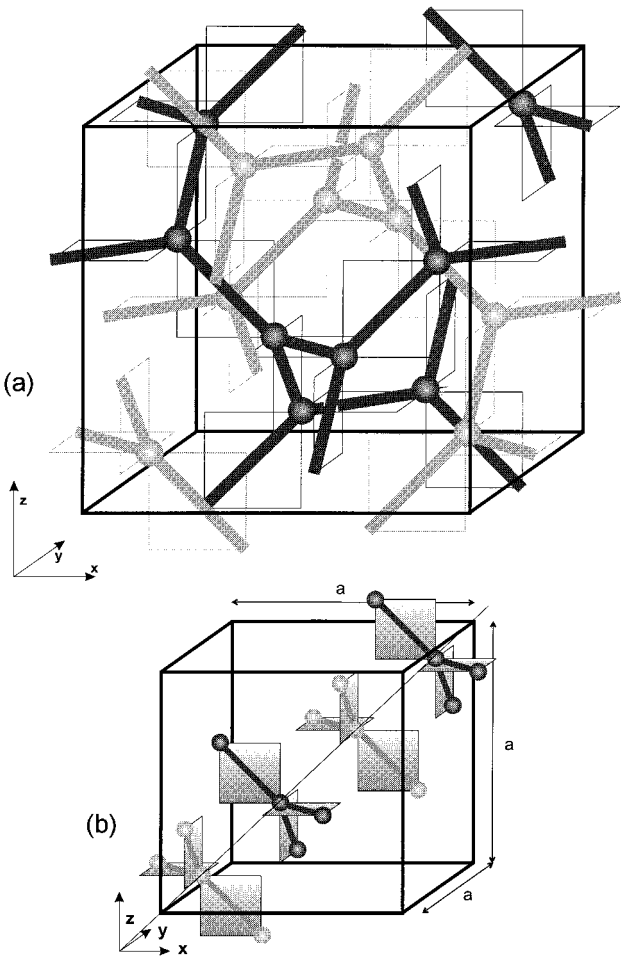


**Figure 16.** Real space morphology of the gyroid phase. (a) The skeleton graph outlining the two interpenetrating networks high in minority component (PDMS) concentration. (b) The 16 symetrically equivalent points with respect to the $Ia\bar{3}d$ space group from which the skeleton graph can be constructed.

## Appendix

**Real Space Structure of the Gyroid Phase.** Originally, "gyroid" is the name of a minimal surface, of $Ia\bar{3}d$ symmetry, that divides the space into two interpenetrating and equally sized volumes.[51] The use of the term in describing the structure associated with the $Ia\bar{3}d$ phase in diblock copolymers was introduced by Hajduk et al.[2] The assignment of the gyroid structure to this PEP−PDMS sample, f69pd, is done by analogy to the real-space morphological studies of other polymer samples,[3,4,10,15,52] displaying scattering and rheology characteristics similar to f69pd. A model of the gyroid structure, based on rod-type connectors,[53] is the skeleton graph, shown in Figure 16a, outlining the core of the two volumes separated by the gyroid minimal surface. Gray and black are used to distinguish between the two skeletal networks, and the dimension of the cubic unit cell, of side length $a$, is also marked in Figure 16a. The interpenetrating networks represent regions of the sample volume where the density of the minority component (i.e., PDMS) is above the average composition ($1 - f_{PEP}$). Likewise, the volume between the networks is of higher density than the majority component (i.e., PEP).

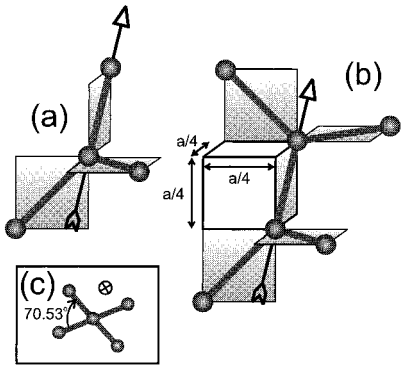


**Figure 17.** Building blocks of the gyroid structure. (a) Connecting one point in space with its three nearest neighbors forms a tripod. (b) Two tripods connect by twisting their planes with respect to each other. (c) The planes are twisted by an angle of 70.53°. Twisting the tripods clockwise results in a "right-handed" network (black in Figure 16a), and twisting the tripods anticlockwise results in a "left-handed" network (gray in Figure 16a).

The skeletal structure can be constructed by connecting the points in space shown in Figure 16b, which are the symmetrically equivalent 16b sites of the $Ia\bar{3}d$ space group.[54] These points map onto themselves with respect to the 3-fold symmetry axis along the [111] direction and the 2-fold symmetry axis parallel with the [1,−2,1] direction through the body center. Figure 16b shows four points on the [111] body diagonal of the unit cube symmetrically positioned around the body center at positions $(3^{1/2}/4)a$ apart. Each of these points is surrounded by three nearest neighbors at a distance of $(\sqrt{2}/4)a$. The nearest neighbors lie in (111) planes separated by 120° angles. By translating the six points outside the cube one cubic lattice unit $a$, all points are inside the cubic unit cell, and the interpenetrating skeleton graph in Figure 16a can be drawn by connecting nearest-neighboring points (at distances $(2^{1/2}/4)a$).

As obvious from Figure 16, the gyroid structure is composed of tripods. One such tripod connector is shown in Figure 17a. The lines connecting the four points of the tripod run across cube faces of side length $^1/_4a$. Two joined tripods are shown in Figure 17b. A close examination of the interconnecting networks show that they have different chirality. When viewed down the connecting line (indicated by an arrow in Figure 17b), the planes spanned by the two tripods are twisted with respect to one another. As illustrated in Figure 17c, the plane of the second tripod is twisted clockwise by 70.53°, which can be calculated by regarding the connecting lines as diagonals of cube faces. The gray network in Figure 16a possess this "right handedness", while the black network in Figure 16a is "left handed".

Figure 18a presents a computer-generated 3D projection of the gyroid structure viewed down the [100] direction. A 2D projection of the structure seen along the $[2\bar{2}0]$ direction with the [111] direction in the plane of the paper is illustrated in Figure 18b. This orientation of the gyroid crystal gives a scattering pattern as shown in Figure 8a-III. The beam direction, the Bragg planes, and the $d$-spacings are marked in Figure 18b. The 2D projection illustrated in Figure 18c along the [111] direction clearly displays the {211}, {220}, and {321} families of crystal planes. This projection comes from Figure 18b by simply rotating the [111] direction from the plane of the paper to point toward the viewer and is a side view of the scattering situation depicted in Figure 18b. The Bragg planes giving the meridional ⟨211⟩ reflections in Figure 8a-III are indicated together with the direction of the incoming beam of neutrons.

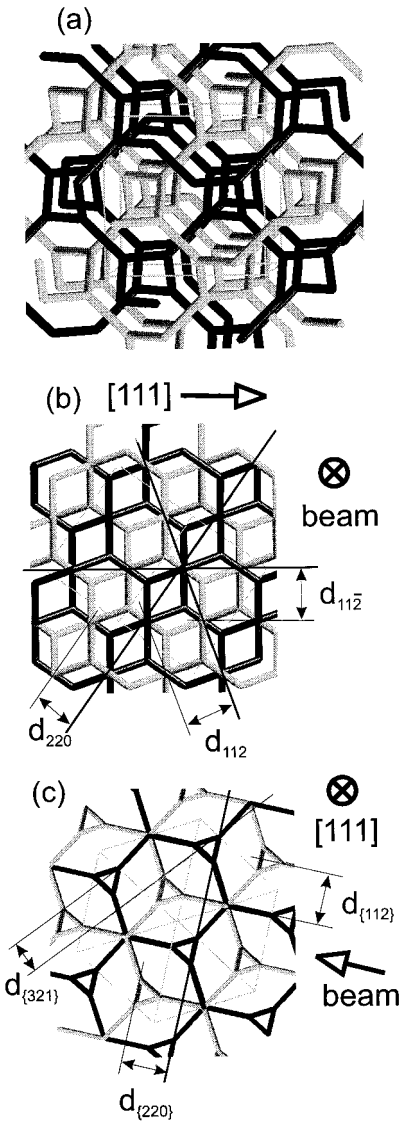


**Figure 18.** Different projections of the gyroid real space structure. (a) A 3D projection seen down the [100] direction. (b) A 2D projection that shows the (112), (112), and (220) Bragg planes causing the scattering pattern illustrated in Figure 8a-IIIa-III. (c) A view along the [111] direction displaying {211}, {220}, and {321} planes.

## References and Notes

(1) Schulz, M. F.; Bates, F. S.; Almdal, K.; Mortensen, K. *Phys. Rev. Lett.* **1994**, *73*, 86.
(2) Hajduk, D. A.; Harper, P. E.; Gruner, S. M.; Honeker, C. C.; Kim, G.; Thomas, E. L.; Fetters, L. J. *Macromolecules* **1994**, *27*, 4063.
(3) Förster, S.; Khandpur, A. K.; Zhao, J.; Bates, F. S.; Hamley, I. W.; Ryan, A. J.; Bras, W. *Macromolecules* **1994**, *27*, 6922.
(4) Khandpur, A. K.; Förster, S.; Bates, F. S.; Hamley, I. W.; Ryan, A. J.; Bras, W.; Almdal, K.; Mortensen, K. *Macromolecules* **1995**, *28*, 8796.
(5) Thomas, E. L.; Lescanec, R. L. *Philos. Trans. R. Soc. London A* **1994**, *348*, 149.
(6) Bates, F. S.; Schulz, M. F.; Khandpur, A. K.; Förster, S.; Rosedale, J. H.; Almdal, K.; Mortensen, K. *Faraday Discuss.* **1994**, *98*, 7.
(7) Seddon, J. M. *Biochim. Biophys. Acta* **1990**, *1031*, 1−69.
(8) Rançon, Y.; Charvolin, J. *J. Phys. Chem.* **1988**, *92*, 2646.

(9) Clerc, M.; Laggner, P.; Levelut, A.-M.; Rapp, G. *J. Phys. Fr. II* **1995**, *5*, 901.
(10) Hajduk, D. A.; Harper, P. E.; Gruner, S. M.; Honeker, C. C.; Thomas, E. L.; Fetters, L. J. *Macromolecules* **1995**, *28*, 2570.
(11) Matsen, M. W.; Schick, M. W. *Phys. Rev. Lett.* **1994**, *72*, 2660.
(12) Matsen, M. W.; Bates, F. S. *Macromolecules* **1996**, *29*, 1091.
(13) Almdal, K.; Mortensen, K.; Ryan, A. J.; Bates, F. S. *Macromolecules* **1996**, *29*, 5940.
(14) Vigild, M. E.; Ndoni, S.; Mortensen, K.; Almdal, K.; Hamley, I. W.; Fairclough, J. P. A.; Ryan, A. J. Phase behaviour of poly(ethylene-alt-propylene)-poly(dimethylsiloxane) (pep-pdms) diblock copolymers., in preparation.
(15) Schulz, M. F.; Khandpur, A. K.; Bates, F. S.; Almdal, K.; Mortensen, K.; Hajduk, D. A.; Gruner, S. M. *Macromolecules* **1996**, *29*, 2857.
(16) Hillmyer, M. A.; Bates, F. S.; Almdal, K.; Mortensen, K.; Ryan, A. J.; Fairclough, J. P. A. *Science* **1996**, *271*, 976.
(17) Podneks, V. E.; Hamley, I. W. *JETP Lett.* **1996**, *64*, 617.
(18) Hamley, I. W.; Podneks, V. E. *Macromolecules* **1997**, *30*, 3701.
(19) Förster, S.; Khandpur, A. K.; Zhao, J.; Bates, F. S.; Hamley, I. W.; Ryan, A. J.; Bras, W. *Macromolecules* **1994**, *27*, 6922. footnote 48.
(20) Hamley, I. W.; Koppi, K. A.; Rosedale, J. H.; Bates, F. S.; Almdal, K.; Mortensen, K. *Macromolecules* **1993**, *26*, 5959.
(21) Hamley, I. W.; Gehlsen, M. D.; Khandpur, A. K.; Koppi, K. A.; Rosedale, J. H.; Schulz, M. F.; Bates, F. S.; Almdal, K.; Mortensen, K. *J. Phys. Fr. II* **1994**, *4*, 2161.
(22) Disko, M. M.; Liang, K. S.; Behal, S. K.; Roe, R. J.; Jeon, K. J. *Macromolecules* **1993**, *26*, 2983.
(23) Pochan, D. J.; Gido, S. P.; Pispas, S.; Mays, J. W. *Macromolecules* **1996**, *29*, 5099.
(24) Hajduk, D. A.; Takenouchi, H.; Hillmyer, M. A.; Bates, F. S.; Vigild, M. E.; Almdal, K. *Macromolecules* **1997**, *30*, 3795.
(25) Fredrickson, G. H. *Macromolecules* **1991**, *24*, 3456.
(26) Hamley, I. W.; Bates, F. S. *J. Chem. Phys.* **1994**, *100*, 6813.
(27) Yeung, C.; Shi, A-.C.; Noolandi, J.; Desai, R. C. *Macromol. Theory Simul.* **1996**, *5*, 291.
(28) Qi, S.; Wang, Z.-G. *Phys. Rev. Lett.* **1996**, *76*, 1679.
(29) Qi, S.; Wang, Z.-G. *Phys. Rev. E* **1997**, *55*, 1682.
(30) Qi, S.; Wang, Z.-G. *Macromolecules* **1997**, *30*, 4491.
(31) Laradji, M.; Shi, A.-C.; Noolandi, J.; Desai, R. D. *Macromolecules* **1997**, *30*, 3242.
(32) Bates, F. S.; Rosedale, J. H.; Bair, H. E.; Russel, T. P. *Macromolecules* **1989**, *22*, 2557.
(33) Brandrup, J.; Immergut, E. H. *Polymer Handbook*, 3rd ed.; John Wiley & Sons: New York, 1989.
(34) Bras, W.; Derbyshire, G. E.; Ryan, A. J.; Mant, G. R.; Felton, R. A.; Lewis, R. A.; Hall, C.; Greaves, G. N. *Nucl. Instrum. Methods Phys. Res.* **1993**, *A326*, 587.
(35) Koppi, K. A.; Tirell, M.; Bates, F. S.; Almdal, K.; Colby, R. H. *J. Phys. Fr. II* **1992**, *2*, 1941.
(36) Kekicheff, P.; Cabane, B. *Acta Crystallogr.* **1988**, *B44*, 395.
(37) Sakya, P.; Seddon, J. M.; Templer, R. H. *J. Phys. Fr. II* **1994**, *4*, 1311.
(38) Zhao, J.; Majumdar, B.; Schulz, M. F.; Bates, F. S.; Almdal, K.; Mortensen, K.; Hajduk, D. A.; Gruner, S. M. *Macromolecules* **1996**, *29*, 1204.
(39) Olsson, U.; Mortensen, K. *J. Phys. Fr. II* **1995**, *5*, 789.
(40) Vigild, M. E.; Almdal, K.; Mortensen, K. Mesoscopic crystallography of the gyroid phase as studied by SANS., to be published.
(41) Almdal, K.; Bates, F. S.; Mortensen, K. *J. Chem. Phys.* **1992**, *96*, 9122.
(42) Bates, F. S.; Koppi, K. A.; Tirrell, M.; Almdal, K.; Mortensen, K. *Macromolecules* **1994**, *27*, 5934.
(43) Koppi, K. A.; Tirrell, M.; Bates, F. S.; Almdal, K.; Mortensen, K. *J. Rheol.* **1994**, *38*, 999.
(44) Tepe, T.; Schulz, M. F.; Zhao, J.; Tirrell, M.; Bates, F. S. *Macromolecules* **1995**, *28*, 3008.
(45) Clerc, M.; Levelut, A. M.; Sadoc, J. F. *J. Phys. Fr. II* **1991**, *1*, 1263.
(46) Stühn, B.; Vilesov, A.; Zachmann, H. G. *Macromolecules* **1994**, *27*, 3560.
(47) Hamley, I. W.; Vigild, M. E.; Almdal, K.; Mortensen, K.; Fairclough, J. P. A.; Ryan, A. J., unpublished results.
(48) Diat, O.; Porte, G.; Berret, J. F. *Phys. Rev. B* **1996**, *54*, 14869.
(49) McConnell, G. A.; Lin, M. Y.; Gast, A. P. *Macromolecules* **1995**, *28*, 6754.
(50) Semenov, A. N. *Macromolecules* **1989**, *22*, 2849.
(51) Schoen, A. H. *NASA Technical Note D-5541*. NASA Washington, DC, 1970.
(52) Spontak, R. J.; Fung, J. C.; Braunfeld, M. B.; Sedat, J. W.; Agard, D. A.; Kane, L.; Smith, S. D.; Satkowski, M. M.; Ashrat, A.; Hajduk, D. A.; Gruner, S. M. *Macromolecules* **1996**, *29*, 4494.
(53) Luzzati, V. *Nature* **1968**, *218*, 1031.
(54) Hahn, T. *International Tables for Crystallography A*; International Union of Crystallography, D. Reidel: Norwell, MA, 1987.

MA9716746